

Internal parameters and regime map for soft polydispersed granular materials

Shunying Ji

*State Key Laboratory of Structural Analysis for Industrial Equipment,
Dalian University of Technology, Dalian 116023 China
and Department of Civil and Environmental Engineering, Clarkson University,
Potsdam, New York 13699*

Hayley H. Shen^{a)}

*Department of Civil and Environmental Engineering, Clarkson University,
Potsdam, New York 13699*

(Received 28 November 2006; final revision received 20 July 2007)

Synopsis

Several internal parameters are studied for a 3D simple shear flow of soft polydispersed granular materials consisting of viscoelastic spheres. These internal parameters include the contact time, the multiple collision group size, and the coordination number. It is found that the contour plots of the contact time and the coordination number in the plane defined by the concentration (solid fraction) and dimensionless stiffness are similar. These contours are qualitatively the same as the regime chart/flowmap proposed in earlier studies. The resulting constitutive relation shows different rate dependency at different concentrations and shear rates. Based on a simple dimensional analysis and a power law formulation, the rate dependency may be expressed by an index. The two extreme values of this index, 0 and 1, correspond to solidlike and gaslike granular materials, respectively. The contour map of this rate index (the power of the dimensionless shear rate in the constitutive relation) resembles those of the λ -shaped curve typical of a phase diagram for ordinary materials. © 2008 The Society of Rheology. [DOI: 10.1122/1.2807441]

I. INTRODUCTION

Ordinary materials exhibit gas, liquid, and solid phases. Transitions between any two phases are controlled by temperature and pressure. Phase transition is well-defined in these thermodynamic equilibrium systems. For granular materials, phenomena analogous to phase transitions have been observed in a variety of geometries, e.g., Couette flows [Savage and Sayed (1984); Hanes and Inman (1985)], inclined flows [Zhang and Campbell (1992); Orpe and Khakhar (2004)]; and channel flows [Hou *et al.* (2003)]. However, lacking a rigorous thermodynamic description, the theoretical basis for transitional phenomena in granular systems is still absent. Because of the dissipative nature, granular materials belong to the category of strongly nonequilibrium systems [Jaeger *et al.*

^{a)}Electronic mail: hhshen@clarkson.edu

(1996)]. A major effort from the theoretical physics community is required to construct a statistical mechanics basis for such systems [e.g., [Edwards et al. \(2005\)](#)].

Because of its dissipative nature, dynamic granular systems must have an energy source from either external vibration or shear. Sheared granular systems are commonplace in many geophysical processes such as sediment transport over land or in a body of water. The pioneer work of [Bagnold \(1954\)](#) described the transition from a “rapid shear” regime to “macroviscous” regime. The stresses, both normal and shear, depend on the square of the shear rate in a rapid shear regime and drops to the first power of shear rate as in a normal Newtonian fluid in the macroviscous regime, when the interstitial fluid becomes dominant. Bagnold’s work for the rapid shear flow was conceptually similar to the kinetic theory of dense gases [[Chapman and Cowling \(1970\)](#)] later adopted to form the kinetic theory of granular flows [[Jenkins and Savage \(1983\)](#)]. Thus the theory for sheared granular materials has been firmly rooted in the fluid mechanics community [[Campbell \(1990\)](#)].

If one takes granular shear flows to the extreme and considers very high solid concentrations encountered in soil mechanics, then it is not difficult to realize that stresses developed inside a granular system can be independent of the shear rate as soil is known to behave as a plastic solid. What controls the transition from a granular gas to a plastic solid in a continuously sheared system? Could a statistical mechanics basis be developed for such systems as well?

In this study, we present a 3D simulation of mildly polydispersed system of soft particles under simple shear. We investigate a number of internal parameters that have been associated with the change of constitutive behavior of sheared granular materials: contact duration, multiple collision group size, and the coordination number. A dimensionless form relating the stresses to the strain rate is given at the end. Using this form, a rate dependency index is introduced to the stresses. The contour plot of this index in the (solid concentration, strain rate)-space provides a regime chart that shows the evolution of granular materials from solidlike to fluidlike phases.

II. PREVIOUS STUDIES

[Babic et al. \(1990\)](#) utilized a discrete element simulation of a 2D system of a simple shear flow of monodispersed viscoelastic disks to study the stresses and shear rate relation. It was found that the dimensionless stress $\tau_{ij}^* = \tau_{ij} / \rho D^2 \dot{\gamma}^2$ depended on the dimensionless shear rate $B = \dot{\gamma} \sqrt{m} / K_n$ in such a way that $\tau_{ij}^* = a_{ij} B^{b_{ij}}$. The parameters a_{ij} and b_{ij} , associated with individual stress components, are both functions of the solid concentration and shear rate. In the above, τ_{ij} is the stress tensor, $\dot{\gamma}$ is the shear rate, ρ is the particle density, D its diameter, m its mass, and K_n its normal stiffness. A more extensive study of this stress-strain rate dependency was later conducted using a 3D assembly of monodispersed spherical particles [[Campbell \(2002\)](#)]. Both the 2D and 3D analyses showed that at very high concentrations the power b_{ij} approached -2 , implies that the dimensional stress τ_{ij} became independent of the shear rate, or the material approached a solidlike state. At very low concentrations, these simulation results confirmed the non-Newtonian behavior, where $b_{ij} \approx 0$ and $\tau_{ij} \approx \dot{\gamma}^2$. It was also found that not only the concentration affected the rate dependency of the stress on the strain rate, but the strain rate itself could also change the power b_{ij} in such way that the higher the strain rate the lower the power b_{ij} .

Based on the simulation observations, including the coordination number, collision frequency and force chain formation patterns, a “regime chart” was speculated to classify the different “regimes” of a granular shear flow. This regime chart is reproduced in Fig.

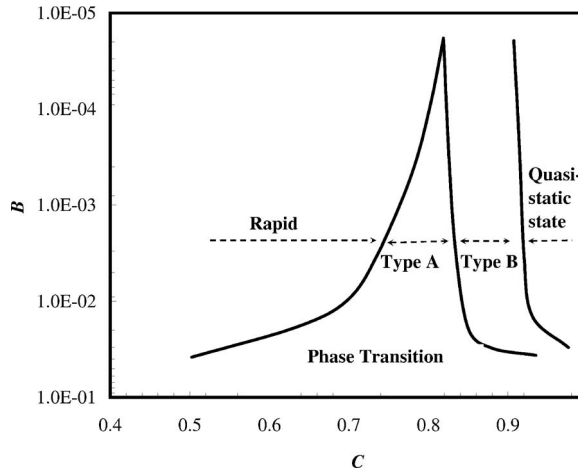


FIG. 1. Flow classification Type A transition refers to multiple collisions, Type B transition refers to force chain formations, and Quasistatic state refers to persistent force chains. The vertical axis $B = \dot{\gamma}\sqrt{m/K_n}$ is the dimensionless shear rate and the horizontal axis is the solid concentration [schematic regime chart, reproduced from Fig. 13 of [Babic et al. \(1990\)](#)].

1 [Fig. 13 of [Babic et al. \(1990\)](#)]. In this figure, “rapid flow” refers to a state where binary collisions are responsible for all stress generation, “Type A” transition refers to multiple collisions “Type B” transition refers to force chain formation, and “quasistaticstate” refers to persistent force chains. In a phenomenological sense, one may associate the rapid flow state with the gaseous phase, the transitional states (A and B) with the liquid phase, and the quasistatic state with the solid phase. The internal processes such as multiple collisions, force chain formation and its persistence, and the shape of the regime chart were postulated without quantitative data.

The existence of such a regime chart was also discovered in a 3D study of monodispersed systems of soft spheres [[Campbell \(2002\)](#)]. A large amount of simulation data from a simple shear flow produced a flowmap [Fig. 10 of [Campbell \(2002\)](#)] of the same shape shown in Fig. 1. In addition, the stress generation mechanisms leading to such transition were also investigated, resulting in different terminology and demarcation criteria for the various phases (inertial-collisional, inertial-noncollisional, elastic-inertial, and elastic-quasistatic). The contact duration was determined and compared with the progression from gaslike to solidlike behaviors. It was found that the dependence of the contact time on the concentration and shear rate closely resembled that of the dimensionless stresses. Because of the differences in the demarcation criteria, the regimes shown in Fig. 1 are only loosely associated with those in [Campbell \(2002\)](#), where the “rapid” regime is split into inertial-collisional and inertial-noncollisional, Type A regime overlaps the inertia-collisional and elastic-inertial, and Type B and quasistatic are combined into elastic-quasistatic regime.

The parameters in a phase diagram such as Fig. 1 are solid concentration and the dimensionless shear rate (or $1/\text{dimensionless particle stiffness}^{1/2}$). These parameters are very different from the familiar thermodynamic parameters of temperature and pressure. Yet the shape of the diagram is strikingly similar to the phase diagram of ordinary materials. We thus ask the question “what are the internal parameters in a granular material that can help us develop an equivalent thermodynamic phase transition theory?”

The contact duration and multiple collision group size were suggested as important

internal parameters in [Babic *et al.* \(1990\)](#). This idea was investigated in [Shen and Sankaran \(2004\)](#) where the stress, shear rate, contact time duration, size of the multiple collision groups, as well as the coordination number were studied for a 2D assembly of soft monodispersed system. Their system was the same as in [Babic *et al.* \(1990\)](#) except that 3000 particles were simulated instead of 30. All phenomena previously discovered were reconfirmed. It was found that indeed the multiple collision size grew with concentration and shear rate. Though not directly measured, when the group size grew to the size of the system, force network must have percolated the whole system, leading to load bearing capacity. Quantifications of the force network by measuring force chain length, density, and their lifetime were not investigated due to the lack of mathematical definitions for these parameters. In addition to the internal length and time scales, the coordination number was also studied. Interestingly, at high shear rates and any concentration, the coordination number appeared to approach a value that corresponded to the coordination number for an isostatic (i.e., statically determinate) system of uniform disks [[Ball \(1999\)](#)].

Recently a 3D discrete element simulation of identical spheres in a simple shear flow was conducted to study the mean contact time and the coordination number in relation to shear rate and solid concentration for a particular granular material with contact friction coefficient of 0.5 and restitution coefficient of 0.7 [[Ji and Shen \(2006\)](#)]. It was found that these two parameters, contact duration and coordination number, seemed to capture the onset of transitional behavior. At a dimensionless mean contact time of ~ 2 , where the dimensionless contact time was defined as the contact time divided by the mean binary contact time, a phase change between a dilute collisional flow and dense transitional flow occurred. At coordination number of ~ 4 phase change between dense transitional flow and quasistatic flow occurred.

To test the robustness of these critical behaviors for more general cases, in this study a 3D simulation is again utilized. Monodispersed systems tend to organize into crystalline structures that may play a role in the behavior of the granular assembly. In this study, we examine a polydispersed system of spheres with a uniform size distribution of $\pm 10\%$ variation from the mean. We include a range of material properties with contact friction $\mu=0.0, 0.1, 0.5$, and 1.0 and restitution $e=0.1, 0.7$, and 1.0 .

III. THE NUMERICAL MODEL

The numerical model follows that of [Babic *et al.* \(1990\)](#); [Campbell \(2002\)](#); and [Shen and Sankaran \(2004\)](#). The contact force between two spherical particles is the sum of a linear spring and a linear dashpot: $F_{spring}=K\delta$ and $F_{dashpot}=\eta\dot{\delta}$, where δ is the particle-particle overlap and $\dot{\delta}$ is the relative velocity of approach between two contacting particles. These two forces act in both the normal and the tangential directions of the contact. A constant relation between the coefficients in the normal and tangential directions are assumed: $K_t=\alpha K_n$, $\eta_t=\beta\eta_n$. In this study we choose $\alpha=1.0$ and $\beta=0.0$, as in the three previous studies cited previously. The tangential force is limited by a friction slider such that the maximum tangential contact force is μ times the normal contact force.

The effective normal stiffness coefficient between two particles A and B, like or unlike, is $K_n=k_n^A k_n^B / (k_n^A + k_n^B)$, where k_n^A and k_n^B are the stiffness coefficients of particles A and B, respectively [[Itasca \(2003\)](#)]. The stiffness in this study is defined as $k_n=\pi DE/4$, where E is the material Young's modulus and D is the particle diameter. (Note: This is the source of the linear contact model. For elastic spheres the true contact stiffness is $K_n=1/3E\sqrt{D}/(1-\nu^2)\delta^{1/2}$, where ν is the Poisson's ratio [[Hertz \(1882\)](#)].) The normal damping coefficient is modeled as $\eta_n=\zeta_n\sqrt{(m_A+m_B)K_n}$, where the dimensionless damping ζ_n is

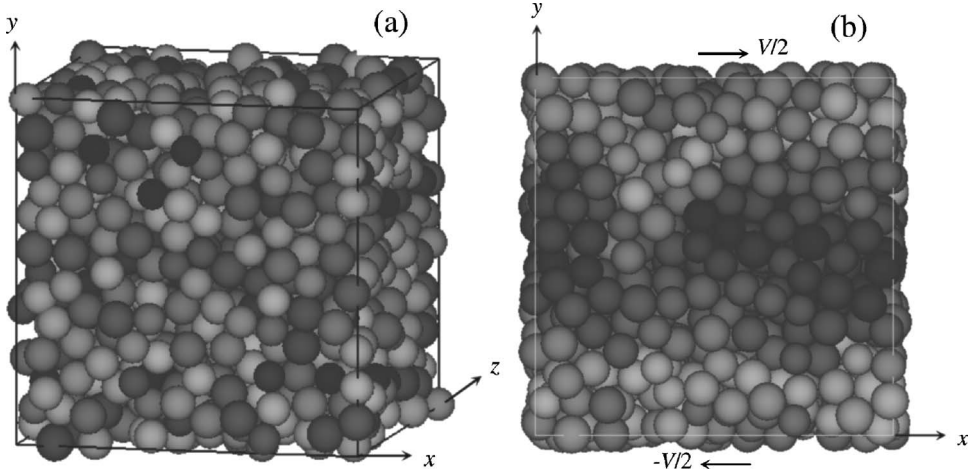


FIG. 2. An example at solid concentration $C=0.7$. (a) Particles packing where darker shading indicates smaller particles, and (b) shear velocity distribution where darker shading indicates slower particles.

defined by the restitution coefficient e as $\zeta_n = -\ln e / \sqrt{\pi^2 + \ln^2 e}$. The macrostresses consist of the contact stress $(1/\nabla)\sum_c D_c k_i^c F_j^c$ and the kinetic stress $(-1/\nabla)\sum_p m_p u_i^p u_j^p$. The summation for the contact stress is over all contact points in the simulation volume and the summation for the kinetic stress is over all particles in the simulation volume. The total stress considered in this study is the sum of these two.

To simulate a simple shear flow we follow the standard techniques developed for nonequilibrium molecular dynamics [Allen and Tildesley (1988)]. The computational domain is first filled with a given number of particles. The velocity V is in the x -direction, with a constant gradient in the y -direction. When one particle moves out from any direction of the computational domain, it re-enters from the opposite direction in the manner explained in Babic *et al.* (1990). In this way, the total granular mass is conserved. To obtain a random packing of polydispersed granular materials at any concentration, a face-centered cubic lattice using the maximum particle size to define the lattice points is adopted. After placing the particles, the domain is expanded or compressed to the desired volume according to the prescribed concentration. During the compression period, the particles rearrange themselves to form a random packing. For low concentrations, expansion of the domain would leave particles in the center portion. Particles in the center portion disperse to fill the domain after shearing starts. All data are obtained after the shearing motion has reached a steady state, as detected by the time series of the stresses.

If the sample size is too small, the boundaries will affect the results. However, the computational cost of increasing the sample size increases rapidly. For a simple shear flow of uniform particles the sample size should be at least $7 \times 7 \times 7$ [Campbell (2002)]. For nonuniform granular materials, boundary effect reduces due to the enhanced disorder from random distributions of particle size and location. In this study, the domain size is chosen to be $a \times b \times c = (10 \times 10 \times 10)\tilde{D}$, where \tilde{D} is the mean particle diameter. In this way, each case has at least $9 \times 9 \times 9$ particles. The steady-state distributions of particle size and velocity in the x -direction for a typical case are shown in Fig. 2. The grayness level in Figs. 2(a) and 2(b) indicates the particle size and velocity, respectively. Shear bands which occurred in monodispersed systems [Babic *et al.* (1990)] are not observed in this study.

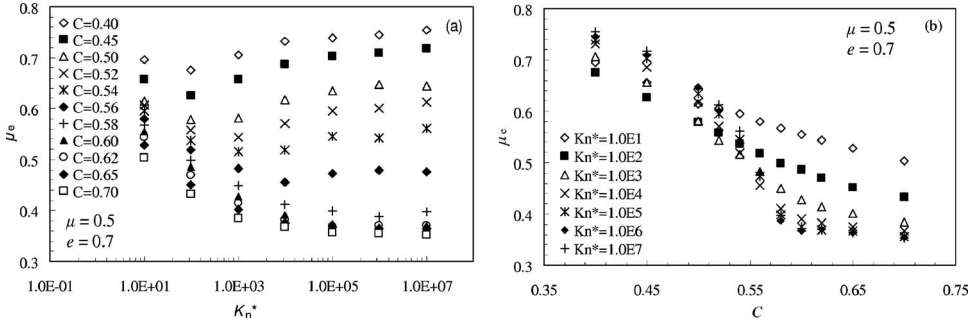


FIG. 3. Effective friction coefficient $\mu_e = \tau_{xy} / \tau_{yy}$ vs dimensionless shear rates and concentrations.

IV. DETERMINATION OF GLOBAL BEHAVIOR

A range of concentration, shear rates, and particle properties including the stiffness, restitution, and friction, are investigated. In this section we present some global properties of the granular assembly, including the stresses and the effective friction defined as $\mu_e = \tau_{xy} / \tau_{yy}$. First, effective friction is presented in Fig. 3. Both Figs. 3(a) and 3(b) use the same data but are plotted in different ways. Figure 3(a) is more conventional, where the effective friction is plotted against the dimensionless stiffness $K_n^* = \tilde{K}_n / \rho \tilde{D}^3 \dot{\gamma}^2$, where \tilde{K}_n is the mean stiffness of the nonuniform particles. The parameter K_n^* is related to the dimensionless shear rate B through $K_n^* = \pi / 6B^2$.

From Fig. 3(a), at high concentrations ($C > 0.58$) the effective friction approaches a constant at large values of K_n^* similar to ordinary frictional solids. However, by investigating the frictional behavior alone it is difficult to determine the state of the granular materials because constant friction is also observed at high K_n^* for concentrations as low as 0.4 where stresses are mainly generated by collisions. Figure 3(b) shows an interesting phenomenon. The friction curves for constant K_n^* intersect. Although the underlying mechanisms are not clear at this point, intersecting curves usually imply that some controlling parameters are at their critical values at the intersection. All curves do not intersect at the same point. For smaller values of K_n^* , the value of C at the intersection is lower.

The stresses themselves are shown in Fig. 4. Unlike the conventional way of presenting the stresses as functions of the shear rate, here the stresses are plotted against the solid concentration. Following Campbell (2002), two different dimensionless forms for the stresses are shown. In semilog plots, the first, defined as $\tau'_{ij} = \tau_{ij} \tilde{D} / \tilde{K}_n$, is strongly sensitive to the shear rate at low concentrations, as shown in Fig. 4(a), and the second, defined as $\tau_{ij}^* = \tau_{ij} / \rho \tilde{D}^2 \dot{\gamma}^2$ is strongly sensitive to the shear rate at high concentrations, as shown in Fig. 4(b). In Fig. 4, $\mu = 0.5$ and $e = 0.7$, and only τ_{xx} is presented. Other stress components behave similarly.

Plotted in this way, it is clear that two distinct mechanisms are at play at different concentrations. From Fig. 4(a), when $C > 0.65$ the curves of $\tau'_{xx} = \tau_{xx} \tilde{D} / \tilde{K}_n$ from all shear rates collapse to one. Hence, the granular materials become an elastic solid. From Fig. 4(b), when $C < 0.4$, the curves of $\tau_{ij}^* = \tau_{ij} / \rho \tilde{D}^2 \dot{\gamma}^2$ collapse to one; hence, the granular materials behave as a kinetic gas where $\tau_{ij} \propto \dot{\gamma}^2$. Somewhere between these two concentrations, phase change must take place. The range of concentration for this transition is expected to depend on the particle's material properties. The same conclusion has been

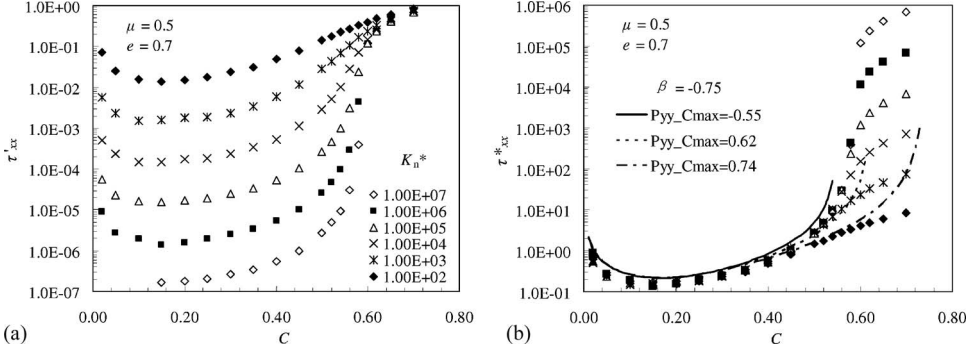


FIG. 4. The relationship between dimensionless stress and shear rate with different concentrations. In (b) the analytic solution from kinetic theory is also included for comparison, in which parameter β is a complex combination of e , μ , and the ratio of tangent to normal velocity at each contact. An average value is used to derive the analytic solution [Lun (1991)]. The choice of $\beta = -0.75$ corresponds to $\mu = 0.5$, $e = 0.7$ and the velocity ratio is 1.

arrived at using the conventional way to plot the dimensionless stresses against the shear rate (as was done for τ'_{ij} versus $1/B^2$ [Campbell (2002)] or for τ_{ij}^* versus B [Babic *et al.* (1990); Campbell (2002)]).

V. INTERNAL PARAMETERS

Phase transition of granular materials is associated with how forces are transmitted within the assembly. Thus, this transition should depend on the material properties at the particle level. It is desirable to determine if there exists a universal parameter(s) that control(s) the transition for all granular materials. In a granular flow, the contact time, the multiple collision group size, the coordination number, and force chains all change significantly during phase transition. Investigating these internal parameters should be the first step toward a quantitative theory for phase transition in a granular material.

The contact time is the most direct measure to distinguish the contact types, which are binary, multiple, or persistent [Zhang and Rauenzahn (1997, 2000); Potapov and Campbell (1996)]. A contact time number may be defined as $m = \bar{T}_c / \tilde{T}_{bc}$, in which \bar{T}_c and $\tilde{T}_{bc} = \pi \tilde{D} / \sqrt{3E(1 - \zeta_n^2) / 2\rho}$ are the mean contact duration and the binary contact time between mean size particles, respectively. When multiple contacts occur, except, very rarely, under high shear rates a third particle may knock a binary collision pair out of contact prematurely, the contact time in general is longer than that in a binary collision, resulting in $m > 1$.

Subtracting the binary contact time from the mean contact time, the net contact time number, defined as $m' = m - 1$ is plotted in Fig. 5. Binary collisions corresponds to $m' = 0$. Figure 5 is for the case $\mu = 0.5, e = 0.7$. The other cases are qualitatively the same. These results are close to the monodispersed case [Fig. 4 of Ji and Shen (2006)]. The appearances of these curves are very similar to those in Fig. 3. That is, relative to K_n^* the curves diverge and relative to C the curves cross. None of the conditions shown correspond to the binary collision case. From Fig. 5(a), for low concentration and low shear rate (large values of K_n^*) the contact duration does approach that of the binary collision. At high shear rates (low values of K_n^*), even for very low concentration binary collision no longer dominates. From Fig. 5(b), the net contact time number increases with concentration but the increasing rates and amplitudes are very different for different shear rates.

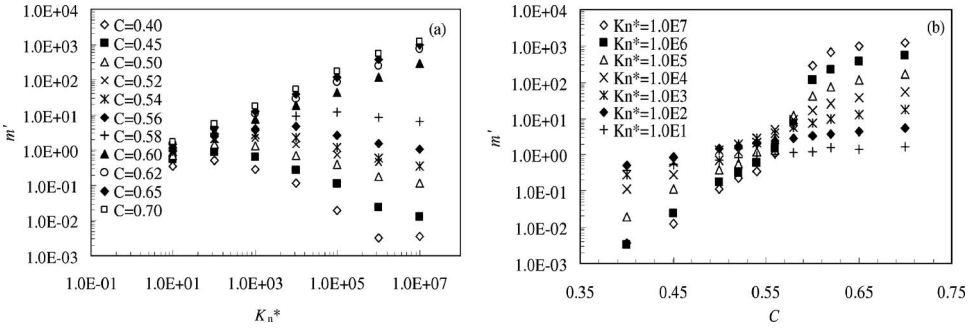


FIG. 5. Contact time number vs (a) dimensionless stiffness and (b) concentration.

These curves intersect within a range of C . If we separate the curves in Fig. 5(b) according to low and high values of K_n^* , as shown in Fig. 6, it is seen that the intersections for low K_n^* are diffused but for high K_n^* all three curves seem to pass through one point where $m' \approx 10$ at $C \approx 0.586$. It is unclear why the nature of these curves should change sharply at certain values of K_n^* . The nature of these intersects also depends on the material properties, as shown in Figs. 7(a) and 7(b) for $\mu=0.5, e=0.1$ and $\mu=1.0, e=0.7$, respectively. More dissipative systems with higher values of friction or lower values of restitution have more diffuse intersections. The case shown in Fig. 7(a) has intersection “point” at $m' \approx 30$ and $C \approx 0.585$. The case shown in Fig. 7(b) is too diffuse to define a single intersection.

To verify that larger values of m' do indeed correspond to multiple collisions leading to load bearing force networks, we examine the spatial characteristics inside a granular material. A “group” defined as the totality of particles connected by a force network was examined in an earlier study to measure the number of simultaneously contacting particles at a given instant [Shen and Sankaran (2004)]. Adopting the same definition, Fig. 8 summarizes the ratio of the maximum group size to the total particle number for the present cases. When this ratio becomes 1, the size of the force networks must span the whole domain. Interestingly, even for concentrations as low as $C=0.4$, the maximum group size reaches nearly 90% of the sample size for very low values of K_n^* (such as $K_n^*=1$). But since the corresponding contact time was only 36% above the binary collision time in this case (Fig. 5), these large force networks are short-lived. This same

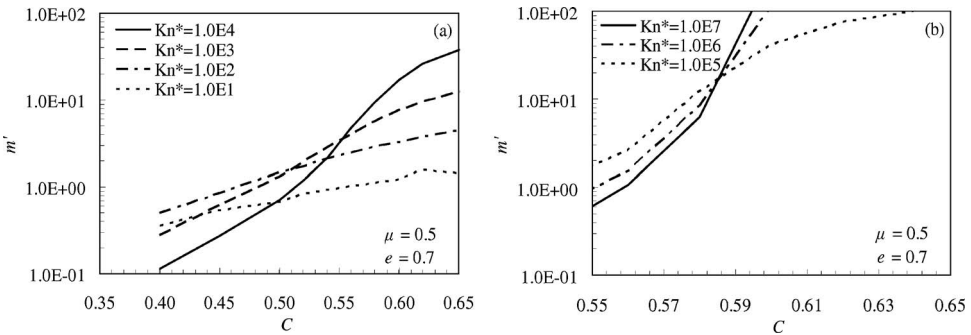


FIG. 6. Intersections of different contact duration curves for (a) low dimensionless stiffness and (b) high dimensionless stiffness.

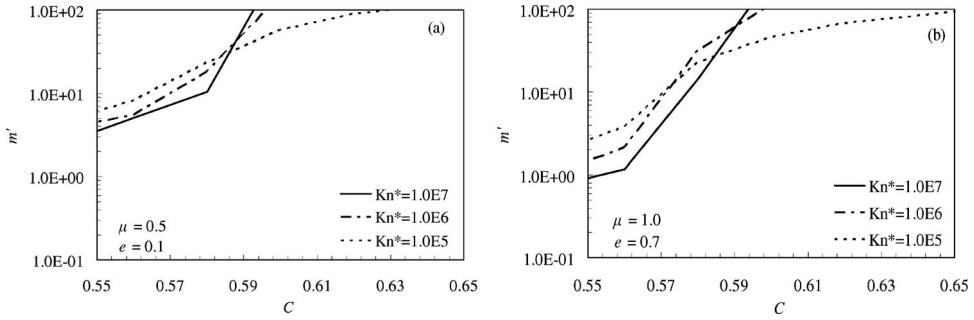


FIG. 7. Intersections of different contact duration curves for different material properties: (a) low restitution and (b) high friction.

observation was made in [Campbell \(2002\)](#). For $C > 0.6$, the maximum group size equals the sample size. Load bearing force networks are present at least part of the time. Unlike the curves of μ_e or m' , these curves do not intersect.

Using pure kinematic constraints, it can be shown that for an isostatic system of monodispersed frictional spheres, the coordination number should be 4 and the corresponding value for disks is 3 [[Ball \(1999\)](#); [Ball and Blumenfeld \(2002\)](#)]. Below this number the assembly is unstable under load and thus should behave as a fluid. For a system of monodispersed disks under simple shear the coordination number was found to approach 3 at high shear rates for $0.8 < C < 0.9$ [[Shen and Sankaran \(2004\)](#)]. Since the critical coordination number was derived from a static equilibrium argument, it is intriguing that the same value can be reached under extremely dynamic conditions. The result of coordination number n for the present study is shown in [Fig. 9](#) for $\mu=0.5, e=0.7$. All other cases are similar. Again, the curves are qualitatively the same as in [Figs. 3 and 5](#): curves relative to K_n^* diverge and relative to C cross.

The crossover point for the n curves is much more sharply defined than the μ_e curves in [Fig. 3](#), and the m' curves in [Fig. 5](#). The intersecting curves are plotted again in [Fig. 10](#) separating the low K_n^* cases from the high K_n^* cases, as in [Fig. 6](#). Very interestingly, it is found that under more dynamic cases (low K_n^* values), the intersections focus at $n=4$, but for less dynamic cases the curves converge at $n \approx 5$ and remain collapsed past this point. It should be pointed out that here the definition of coordination number is $2 \times$ number of contact/number of particles. In [Ball and Blumenfeld \(2002\)](#), particles with one contact or

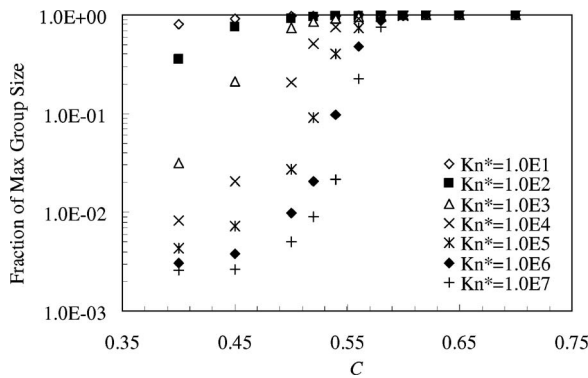


FIG. 8. Particle group size vs shear rates and concentrations.

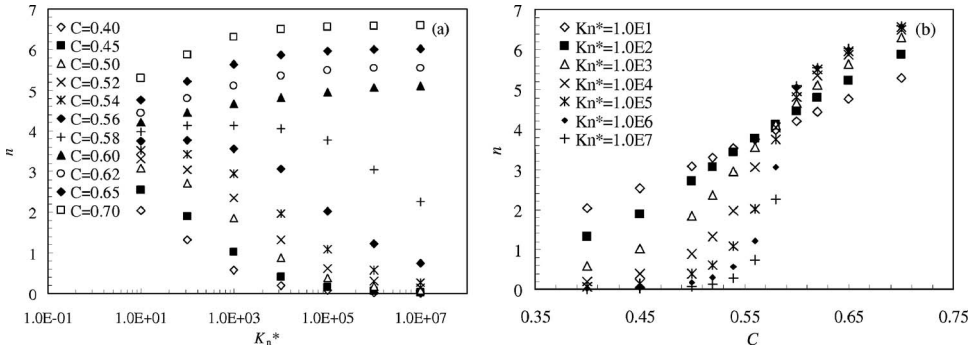


FIG. 9. Coordination number versus (a) shear rates and (b) concentrations.

no contact were excluded from the averaging, as defined in Thornton (2000). As the solid concentration decreases, the differences between these two definitions may be important.

We investigate the effects of restitution and friction in Fig. 11. Restitution does not change the previously mentioned observations for the coordination number, but friction does. At higher friction, the intersection of high K_n^* curves are moved to higher values of n . But the more dynamic cases still seem to maintain the $n=4$ intersection. The significance of this apparently robust parameter is unknown. As discussed in Campbell (2002), friction helps to sustain force chains and thus it is expected that coordination number increases with increasing friction.

A more concise way to represent the coordination number is by plotting its contours with respect to the concentration C and the dimensionless stiffness K_n^* . These plots are shown in Fig. 12 for the cases $\mu=0.0, 0.1, 0.5, 1.0$ and $e=0.1, 0.7, 1.0$. If there exists a real critical value of the coordination number, then one of the contours must be a straight vertical line. Along this line the coordination number is a constant with respect to the shear rate or particle stiffness. The corresponding concentration is thus the critical concentration, below which we may call the system a quasifluid and above which a quasisolid. The prefix “quasi” emphasizes the fact that some rate dependency remains no matter how “solidlike” and some load bearing force chains may instantaneously exist no matter how “fluidlike” the granular assembly is. In each case shown in Fig. 12, one contour closely approaches vertical for a broad range of $K_n^* \geq 10^4$, indicating no rate

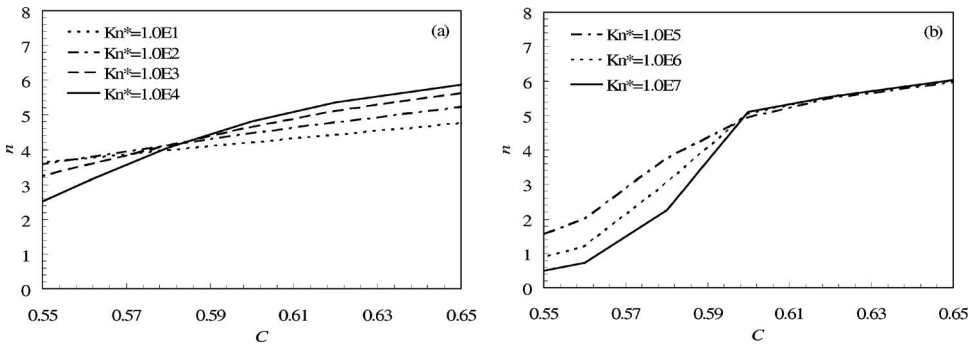


FIG. 10. Details of the intersecting curves of the coordination number (a) low dimensionless stiffness and (b) high dimensionless stiffness.

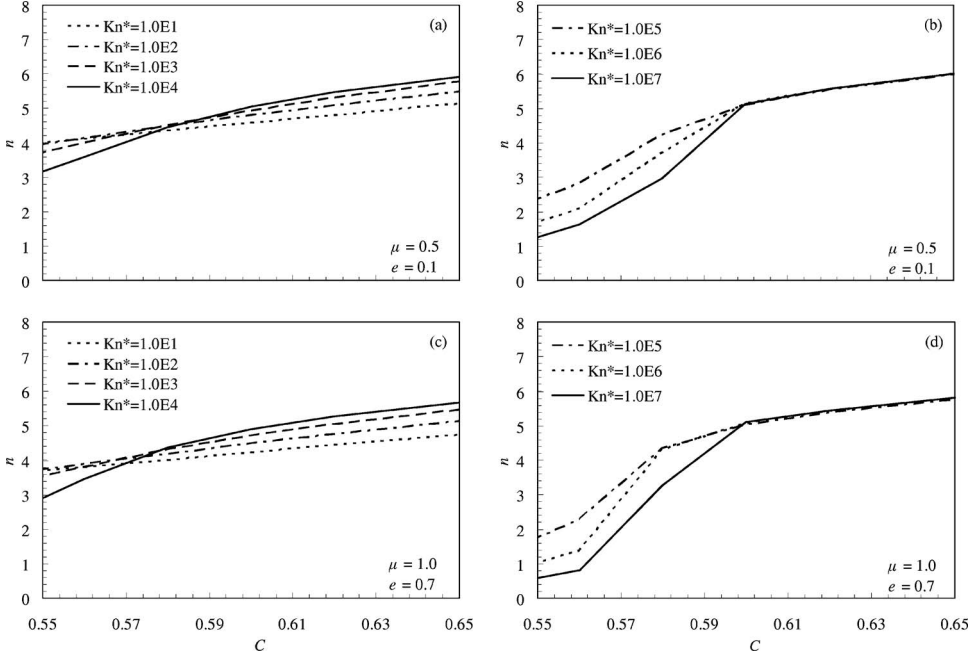


FIG. 11. Details of the intersecting curves of the coordination number (a) and (b) low restitution and (c) and (d) high friction.

dependency at the corresponding concentration. At either side of this concentration, a qualitative change of the constitutive relation is expected. The contour value for the curve closest to vertical varies between 4 and 5 for the cases studied.

VI. CONSTITUTIVE RELATIONS

To investigate how constitutive relations change corresponding to the previous internal parameters, we express the stress components as follows [Babic *et al.* (1990); Campbell (2002)];

$$\tau_{ij} = f_{ij}(\dot{\gamma}, C, D, \rho, K_n, \mu, e). \quad (1)$$

For the polydispersed granular materials, the mean particle diameter \tilde{D} and mean stiffness \tilde{K}_n replace D and K_n in Eq. (1). Using the dimensionless stress $\tau_{ij}^* = \tau_{ij} / \rho \tilde{D}^2 \dot{\gamma}^2$ and dimensionless stiffness $K_n^* = \tilde{K}_n / \rho \tilde{D}^3 \dot{\gamma}^2$, Eq. (1) can be written as

$$\tau_{ij}^* = f_{ij}^*(K_n^*, C, \mu, e). \quad (2)$$

From the observed stress and shear rate relation a simple power law is suggested as

$$\tau_{ij}^* = a_{ij}(K_n^*)^{b_{ij}}, \quad (3)$$

where $a_{ij} = a_{ij}(C, \mu, e)$ and $b_{ij} = b_{ij}(C, \mu, e)$. The parameters, a_{ij} and b_{ij} , are associated with respective individual stress components. As will be shown next, both a_{ij} and b_{ij} vary slowly with K_n^* . Substituting $\tau_{ij}^* = \tau_{ij} / \rho \tilde{D}^2 \dot{\gamma}^2$ and $K_n^* = \tilde{K}_n / \rho \tilde{D}^3 \dot{\gamma}^2$ into Eq. (3), we obtain the constitutive equation of granular materials as

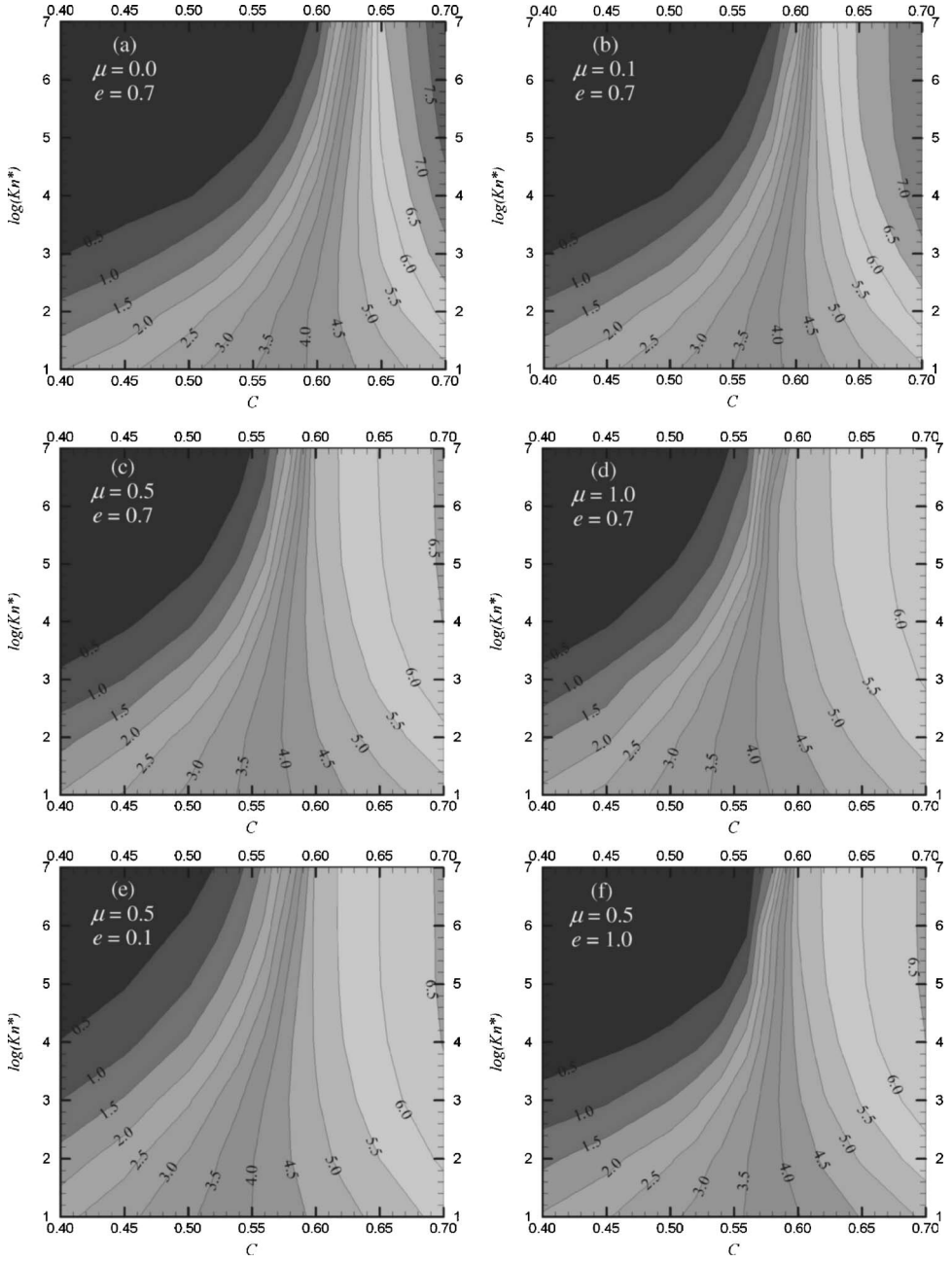


FIG. 12. Contours of coordination number. In all cases the contours begin with the value of 0.5 from the left at intervals of 0.5.

$$\tau_{ij} = a_{ij} \tilde{K}_n^{b_{ij}} (\rho \dot{\gamma}^2)^{1-b_{ij}} \tilde{D}^{2-3b_{ij}} \quad \text{or} \quad \tau_{ij} = a_{ij} \tilde{K}_n^{1-c_{ij}} (\rho \dot{\gamma}^2)^{c_{ij}} \tilde{D}^{3c_{ij}-1}. \quad (4)$$

When b_{ij} approaches 1, the stress is rate independent and when b_{ij} approaches 0 the stresses agree with the kinetic theory. A rate dependency index $0 < c_{ij} = 1 - b_{ij} < 1$ is thus

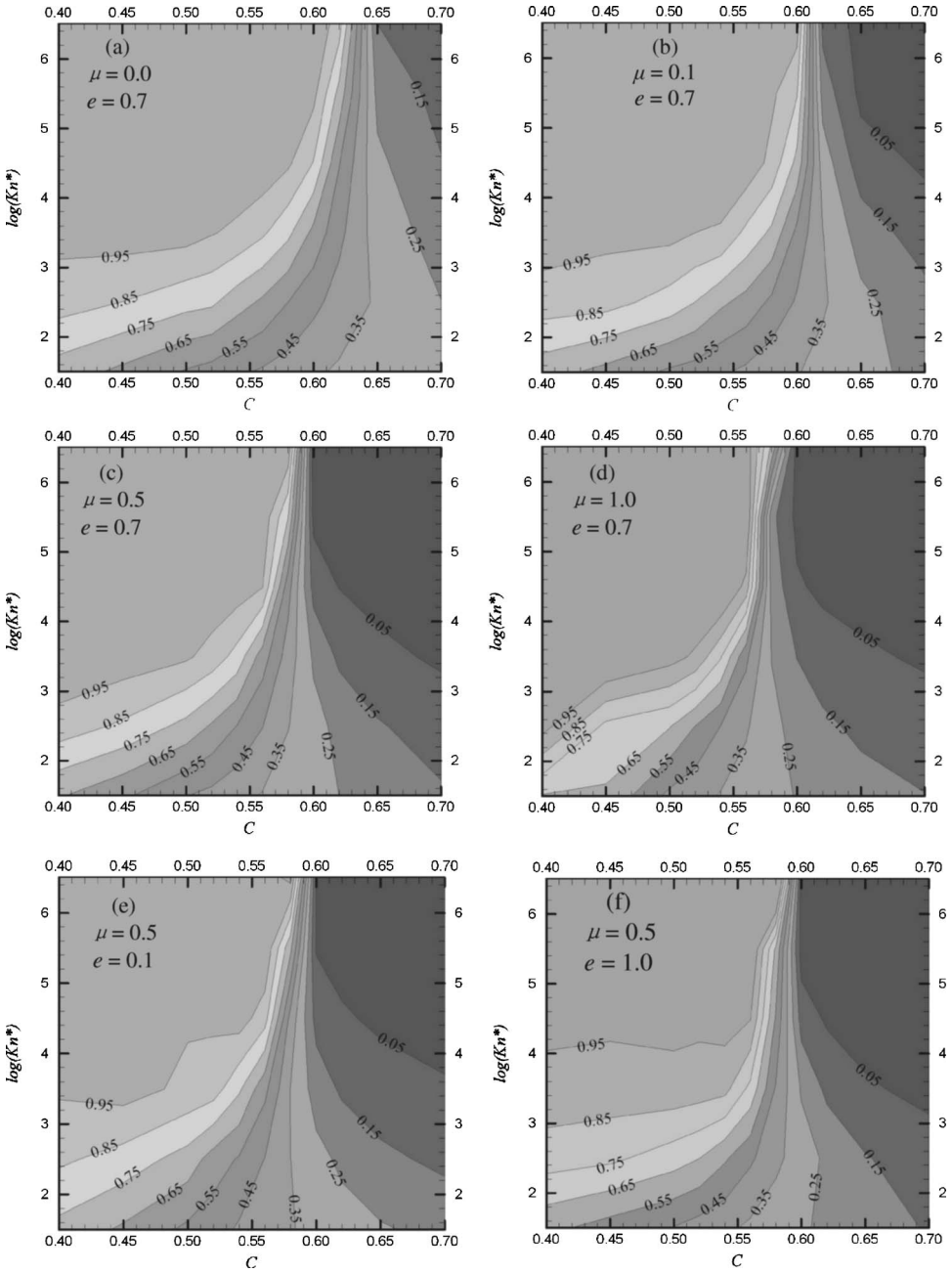


FIG. 13. Contour of c_{xy} in the constitutive model. All contours begin with the value of 0.95 from the left with an interval of 0.1.

defined. The higher the value of c_{ij} the more kinetic gas-like the stress is. Figure 13 shows the contours of c_{ij} for the cases studied.

Figure 13 is directly related to the rate dependency of the granular materials and thus represents the most important measure of the different phases; the higher the index c_{ij} , the more fluidlike the granular material. From these contours it is clear that some rate de-

pendency exists for most cases studied. Contact friction and restitution do not seem to impact these contours significantly, except for low values of friction.

VII. DISCUSSION

Two of the internal parameters studied, contact time number and coordination number, demonstrate the same behavior. That is, when plotted against the dimensionless stiffness (or $1/\text{dimensionless shear rate}^2$), they diverge, and when plotted against concentration they cross. The same phenomenon is present in the effective friction μ_e (Fig. 3). Crossing of a family of curves implies the existence of some critical value corresponding to a change of material behavior. The possibility of critical values is investigated in terms of the contact time and the coordination number.

The contour plots of the coordination number are similar to the regime chart in [Babic et al. \(1990\)](#) and the flowmap in [Campbell \(2002\)](#), although in these two earlier studies no specific quantity was used to define the boundaries between different types of granular shear flows. What we have found in this study is that not only the coordination number follows the type of phase change-like behavior, but the contact duration also follows the exact same trend (with similar contours). Some bulk properties, such as the effective friction, behave the same as well. The rate dependency index c_{ij} is the most important parameter that describes the constitutive properties of a granular material. When it approaches 1, the material follows the same constitutive relation as a kinetic gas. When it approaches 0, the material is a frictional solid. The contour plots of c_{ij} are qualitatively the same as those of the contact duration, the coordination number, and the bulk friction. (Of the three, only those of the coordination number are shown.) When we compare Fig. 12(c) and Fig. 13(c) in the region where $c_{xy}=0$, indicating a solid behavior, the coordination number varies between 5 and 6.5. This shows that coordination number alone does not capture the phase change behavior. The same can be said for other internal parameters.

From Fig. 13 a family of λ -shaped curves exists that describes the transition from a dilute flow where stresses are generated by particle inertia (a gaslike phase), to multiple collisions and occasional force chain formation (a liquidlike phase), to finally persistent force chain formation with load bearing capability and negligible rate dependence (a solidlike phase). Unlike ordinary materials with well defined boundaries between different phases, this family of λ -shaped curves is diffuse with many contours between solidlike and fluidlike regimes. The “phase change” in granular materials is not through discontinuous change of any parameters, at least in terms of those currently considered.

We began our study by asking whether there exist internal parameters that can help us develop an equivalent thermodynamic phase transition theory for a granular material. After examining three internal parameters of contact time, multiple collision group size, and the coordination number, we find that a “quasiphase transition” does exist, but its relation with thermodynamic type of parameters is not yet developed. The current parameters for constitutive relations in a granular material, C and K_n^* , are from simple dimensional analysis. While one may argue that pressure and granular temperature are direct manifestations of C and K_n^* , the relation between the stress and shear rate has not been expressed in terms of those more familiar thermodynamic variables.

Even in the absence of a clear phase diagram, the contours of c_{ij} provide a relatively complete picture of how granular materials change their constitutive behavior.

The result concerning coordination number is the most interesting of all. Of all the internal parameters studied here, coordination number has the most distinct critical behavior, although not a unique point, when plotted against C (Fig. 12). The contour plots

are also the closest to the contours of c_{ij} . The fact that the critical values of the coordination number seem to approach the value predicted from isostatic granular materials (and of uniform particle size) is intriguing. For different values of contact friction and restitution, the critical coordination number is not a constant but varies between 4 and 5 in the currently studied systems.

It is worthwhile commenting on the limiting case when $c_{ij} \rightarrow 0$. From Eq. (4) this would lead to $\tau_{ij} \rightarrow a_{ij} \tilde{K}_n \tilde{D}^{-1}$ and thus appears to be singular as $\tilde{D}^{-1} \rightarrow 0$. In fact, to facilitate a linear spring contact model, the spring constant is related to the particle's Young's modulus $\tilde{K}_n \approx E\tilde{D}$. Hence, in the limiting case, Eq. (4) reduces to $\tau_{ij} \approx a_{ij}E$ and is bounded.

Throughout the discussion in this work, the significance of one important internal parameter, namely the force chain, has been frequently implied. However, despite abundant reports on the observations of force chains in a shearing granular material, both experimentally or via computer simulations [De Josselin de Jong and Verruijt (1969); Cundall and Strack (1979); Oda *et al.* (1980); Behringer *et al.* (1999)], an attempt to rigorously define them and to relate them to mechanical properties of the granular assembly is very recent [e.g., Goldenberg and Goldhirsch (2002)]. A quantitative description of force chain dynamics has yet to be developed. Some initial attempts to mathematically define a force chain have begun [Peters *et al.* (2005); Muthuswamy and Tordesillas (2006)]. On the other hand, the contact time and its dynamics have been described in statistical mechanics terms [Zhang and Rauenzahn (1997, 2000)].

Finally, all data produced in this study are from a viscoelastic contact law with a single friction coefficient. Other contact laws can also model dissipative granular systems. In particular, elastoplastic contacts has also been adopted to fit a given restitution coefficient [Thornton (1997)]. However, unlike the viscoelastic particles, for elastoplastic contacts the contact duration decreases when the restitution decreases. Consequently, when comparing results between different dissipative systems, it is important to know the exact nature of the dissipation. Likewise, if both static and dynamic frictions are included in the model, complex stick-slip conditions can result at the microlevel. In depth study of the effect of contact mechanics on the transition of granular materials is desirable.

VIII. CONCLUSIONS

We used a 3D simulation of soft polydispersed spheres to study the transitional behavior of a simple shear granular material. Previously we found that for a simple shear flow of monodispersed system, the contact time and the coordination number in a $C - K_n^*$ space produced contours similar to the regime chart/flowmap proposed from phenomenological considerations in earlier studies. In this study, we examined polydispersed systems and a range of material properties. It has been confirmed that the contact time and the coordination number both behave similarly with respect to the solid concentration and the shear rate. A relatively sharp transition between solidlike and gaslike phases exists for low shear rates, when concentration varies from high to low. At high shear rates, a more gradual transition exists between solidlike and gaslike phases when concentration reduces. The fluidlike state is broadly defined in such way that the stresses are dependent on the shear rate, including the extreme case when kinetic theory applies and the granular material is in the kinetic gas phase.

Realization of dimensionless shear rates as high as required to experience a broad range of rate dependency via varying concentration requires soft materials. For most geological materials on earth, the dimensionless shear rate lies in the top part of the

contour map shown in Figs. 12 and 13. Thus transitions from a quasistatic solid phase to that of the kinetic gas phase are relatively sharp as discovered by other researchers [Aharonov and Sparks (1999); Campbell (2002)].

A power law constitutive model is developed in which $\tau_{ij} = a_{ij} \tilde{K}_n^{1-c_{ij}} (\rho \dot{\gamma}^2)^{c_{ij}} \tilde{D}^{3c_{ij}-1}$. The contours of the rate index c_{ij} are similar to those of the coordination number. These regime maps are not phase diagrams of the normal thermodynamic type because the variables used are not the ordinary thermodynamic quantities.

It is clear that there is a lot more to be studied concerning the transition of granular materials. What we have found that has further complicated the matter is that the contour map of the rate index differs for different stress components. What this means for definitions of phase change remains to be seen. Nonetheless, this study shows how several internal parameters behave very similarly during transition. It is hopeful that by studying these parameters and their relations, a theoretical basis may be constructed for the transition process in granular materials.

ACKNOWLEDGMENTS

Comments from James T. Jenkins were deeply appreciated. This study was supported by the NASA Microgravity Fluid Physics Program (Grant No. NAG3-2717).

References

- Allen, M. P., and D. J. Tildesley, *Computer Simulation of Liquids* (Oxford University Press, New York, 1988), p. 385.
- Aharonov, E., and D. Sparks, "Rigidity phase transition in granular packings," *Phys. Rev. E* **60**, 6890–6896 (1999).
- Babic, M., H. H. Shen, and H. T. Shen, "The stress tensor in granular shear flows of uniform, deformable disks at high solids concentrations," *J. Fluid Mech.* **219**, 81–118 (1990).
- Bagnold, R. A., "Experiments on a gravity-free dispersion of large solid spheres in a Newtonian fluid under shear," *Proc. R. Soc. London, Ser. A* **225**, 49–63 (1954).
- Ball, R. C., "The propagation of stress through static powders, in Structures and dynamics of materials in the mesoscopic domain," edited by M. Lal, R. A. Mashelkar, B. D. Kulkarni, and V. M. Naik (Imperial College Press, London, 1999), pp. 326–339.
- Ball, R. C., and R. Blumenfeld, "Stress field in granular systems: loop forces and potential formation," *Phys. Rev. Lett.* **88**, 115505 (2002).
- Behringer, R. P., D. Howell, L. Kondic, S. Tennakoon, and C. Veje, "Predictability and granular materials," *Physica D* **133**, 1–17 (1999).
- Campbell, C., "Rapid granular flows," *Annu. Rev. Fluid Mech.* **22**, 57–92 (1990).
- Campbell, C., "Granular shear flows at the elastic limit," *J. Fluid Mech.* **465**, 261–291 (2002).
- Chapman, S., and T. G. Cowling, *The Mathematical Theory of Non-Uniform Gases*, 3rd Ed. (Cambridge University Press, New York, 1970).
- Cundall, P. A., and O. D. L. Strack, "A distinct element model for granular assemblies," *Geotechnique* **29**, 47–65 (1979).
- De Josselin de Jong, G., and A. Verrijdt, "Etude photo-élastique d'un empilement de disques," *Cah. Groupe Fr. Rheol.* **2**, 73–86 (1969).
- Edwards, S. F., J. Brujic, and H. A. Makse, "A basis for the statistical mechanics of granular systems," e-print arXiv:cond-mat/0503057v1 (2005).
- Goldenberg, C., and I. Goldhirsch, "Force chains, microelasticity, and macroelasticity," *Phys. Rev. Lett.* **89**, 084302 (2002).
- Hanes, D. M., and D. L. Inman, "Observations of rapidly flowing granular-fluid materials," *J. Fluid Mech.* **150**,

- 357–380 (1985).
- Hertz, H., “Über die Berührung fester elasticcher Körper (On the contact of elastic solids),” *J. Reine Angew. Math.* **92**, 156–171 (1882).
- Hou, M., W. Chen, T. Zhang, K. Lu, and K. Chan, “Global nature of dilute-to-dense transition of granular flows in a 2D channel,” *Phys. Rev. Lett.* **91**, 204301 (2003).
- Itasca Consulting Group, Inc., ICG, *PFC3D (Particle Flow Code in 3 Dimension)*, Version 3.0, Minneapolis, MN (2003).
- Jaeger, H. M., S. R. Nagel, and R. P. Behringer, “Granular solids, liquids, and gases,” *Rev. Mod. Phys.* **68**, 1259–1273 (1996).
- Jenkins, J. T., and S. B. Savage, “A theory for the rapid flow of identical, smooth, nearly elastic, spherical particles,” *J. Fluid Mech.* **130**, 187–202 (1983).
- Ji, S., and H. H. Shen, “Characteristics of temporal-spatial parameters in quasi-solid-fluid phase transition of granular materials,” *Chin. Sci. Bull.* **51**, 646–654 (2006).
- Lun, C. K. K., “Kinetic theory for granular flow of dense, slightly inelastic, slightly rough spheres,” *J. Fluid Mech.* **233**, 539–559 (1991).
- Muthuswamy, M., and A. Tordesillas, “How do interparticle contact friction, packing density and degree of polydispersity affect force propagation in particulate assemblies,” *J. Stat. Mech.: Theory Exp.* DOI: 10.1088/1742-5468/2006/09/P09003 (2006).
- Oda, M., J. Konishi, and S. Nemat-Nasser, “Some experimentally based fundamental results on the mechanical behavior of granular materials,” *Geotechnique* **30**, 479–495 (1980).
- Orpe, A. V., and D. V. Khakhar, “Solid-fluid transition in a granular shear flow,” *Phys. Rev. Lett.* **93**, 068001 (2004).
- Peters, J. F., M. Muthuswamy, J. Wilbowo, and A. Tordesillas, “Characterization of force chains in granular material,” *Phys. Rev. E* **72**, 041307 (2005).
- Potapov, A. V., and C. S. Campbell, “Computer simulation of hopper flows,” *Phys. Fluids* **8**, 2884–2894 (1996).
- Savage, S. B., and M. Sayed, “Stresses developed by dry cohesionless granular materials sheared in an annular shear cell,” *J. Fluid Mech.* **142**, 391–430 (1984).
- Shen, H. H., and B. Sankaran, “Internal length and time scales in a simple shear granular flow,” *Phys. Rev. E* **70**, 051308 (2004).
- Thornton, C., “Coefficient of restitution for collinear collisions of elastic-perfectly plastic spheres,” *J. Appl. Mech.* **64**, 383–386 (1997).
- Thornton, C., “Numerical simulations of deviatoric shear deformation of granular media,” *Geotechnique* **50**, 43–53 (2000).
- Zhang, D. Z., and R. M. Rauenzahn, “A viscoelastic model for dense granular flows,” *J. Rheol.* **41**, 1275–1298 (1997).
- Zhang, D. Z., and R. M. Rauenzahn, “Stress relaxation in dense and slow granular flows,” *J. Rheol.* **44**, 1019–1041 (2000).
- Zhang, Y., and C. S. Campbell, “The interface between fluid-like and solid-like behavior in two-dimensional granular flows,” *J. Fluid Mech.* **237**, 541–568 (1992).